# ESTIMATION OF 3-D DEFORMATION FROM ONE OR MORE IMAGES WITH WEAK IMAGING GEOMETRY

Olli Jokinen and Henrik Haggrén

Aalto University School of Engineering, Department of Surveying, Finland

olli.jokinen@aalto.fi, henrik.haggren@aalto.fi

## *ABSTRACT*

*The paper proposes a new method for estimation of 3-D deformation of an object from a single image or from multiple images in fixed positions with weak imaging geometry. It is assumed that the 3-D coordinates of the object points before deformation and the 2-D image coordinates after deformation are available and the interior and exterior orientations of the images are known. The core of the method is to approximate the 3-D deformation by a suitable shape function containing parameters the values of which are estimated during adjustment. Experimental results prove high accuracy and fast computing time of the proposed method in cases where the traditional method fails. The proposed method is mainly intended for applications where restrictions set by the measurement environment hinder obtaining strong imaging geometry and where some knowledge of the type of deformation that is likely to occur is available.*

## 1. INTRODUCTION

We consider the case where one or more cameras mounted in fixed positions monitor an object which experiences a deformation. It is assumed that there appear distinguishable target points on the object surface which can be measured accurately from the images. The objective is to measure the 3-D deformation of the object using the image observations of the target points. The traditional way to solve the problem is to compute 3-D coordinates from the measured image coordinates of multiple images before and after deformation separately and then to calculate the difference between the observed 3-D coordinates (Hinz *et al.*, 2007; Liu *et al.*, 2010; Orteu, 2009; Peipe *et al.*, 2006; Tournas *et al.*, 2006). This requires that we firstly have several cameras and secondly that the imaging geometry is appropriate, i.e., the intersection angles between the image rays of corresponding points are large enough (but not too large, however). In many practical situations, however, it may be difficult or even impossible to place the cameras optimally due to restrictions set by the measurement environment. Such cases include, e.g., monitoring a target point at the end of a long narrow corridor. Weak imaging geometry then yields inaccurate results for the estimated deformation.

In this paper, we propose a novel approach where the 3-D deformation is estimated directly from the image observations of a single or multiple cameras with known interior and exterior orientations without computing the actual 3-D coordinates after deformation. Only the 3-D coordinates before deformation and the 2-D image coordinates after deformation are needed. The 3-D coordinates before deformation are obtained from a known reference model of the object assumed to be available. In fact, in many quality control applications there is available a designed model of the object and the task is to measure deviations between the actual and designed shape of the object.

Our solution for estimation of 3-D deformation is based on a suitable shape function introduced for the 3-D deformation. The shape function includes parameters the values of which are estimated during adjustment. The motivation for our approach is that in many close-range applications, the shape of deformation is often smooth with no abrupt changes so that it can be described using continuously differentiable functions such as polynomials. It will be shown that estimation of deformation is possible even if the imaging geometry is weak and further, even from a single image with the help of a shape function. Knowledge of the functional form of the deformation that is expected occur, is assumed known. Such knowledge may be obtained, e.g., from analytical calculations, numerical simulations, or previous experience on similar situations.

There appear only a few related papers in literature dealing with weak imaging geometry, e.g., when the physical environment restricts the placement of target points monitored. In (Fraser and Riedel, 2000), the deformation of steel beams is monitored when the beams cool from very hot to room temperature. Special ceramic targets subject to positional displacement are attached to the beams and several stable reference points are placed behind the thermal testing pit. The stable points provide a fixed reference system from epoch to epoch and a necessary broad spread of monitoring points to support photogrammetric bundle adjustment. The adjusted network comprises all image coordinate observations recorded up until that point so that the stable points are common to all epochs whereas the targets on the beam are re-labeled and thus constitute new object points at each epoch.

The deformation may be also constrained to a particular direction. Such a case is studied in (Jiang and Jauregui, 2010), where the vertical deflection of a bridge under load is measured photogrammetrically. Three reference target points placed on tripods are leveled to the same elevation defining thus a horizontal plane and the plumb vertical direction. It is shown that this approach of defining the reference coordinate system gives similar measurement accuracy as the conventional method where reference control points are placed all around the object space. It is also pointed out that self-calibration of the camera improves the measurement accuracy.

Estimation of 3-D deformation from a single image is an ill-posed problem but it can be solved if some additional information is available. In (Leotta, 2010), a deformable vehicle model is fitted to image observations using edges as model primitives and reducing the number of estimated parameters by principal component analysis. Chen *et al.* (2010) consider using the silhouette to infer the 3-D shape of a deformable object from a single image. In (Albert *et al*., 2002), the deformation is constrained to a plane parallel to the image plane so that the magnitude of deformation is directly proportional to the change in the image coordinates. Taddei and Bartoli (2008) deal with isometric deformations of a paper-like surface with a constraint that the rulings of the paper remain parallel. The problem is shown to be equivalent to the reconstruction of a 2-D curve seen from a set of 1-D camera pairs, which can be solved using a single image.

High accuracy for the deformation measurement can be obtained if the imaging geometry is strong. Tyson *et al.* (2002) report accuracies of 1:30000 of the field of view while in (Maas, 1998), a precision of 1:100000 of the object dimensions is obtained when the 3-D coordinates of the target points and the interior and exterior orientations of the images are solved in a self-calibrating bundle adjustment. We will show that high accuracy can be achieved also for weak imaging geometry if the shape functions for the deformation are correctly selected.

The paper is organized as follows. The new method based on a shape function is presented in Section 2. The method is experimentally validated and compared to the traditional method in Section 3. Conclusions are presented in Section 4.

## 2. NEW METHOD FOR DEFORMATION ESTIMATION

Assume that we have a set of points $(X_i, Y_i, Z_i), i = 1,\ldots,N,$ given on the model surface of the object in the object coordinate system. When the object experiences a deformation, the points move to $(X_i + \Delta X_i, Y_i + \Delta Y_i, Z_i + \Delta Z_i)$. An image is captured after deformation. The well-known collinearity equations relate the deformed object coordinates to the image coordinates $(x_i', y_i')$ corrected from lens distortions and centered at the principal point as follows

$$\begin{aligned} x_i' &= -c\frac{R_{11}(X_i + \Delta X_i - X_0) + R_{12}(Y_i + \Delta Y_i - Y_0) + R_{13}(Z_i + \Delta Z_i - Z_0)}{R_{31}(X_i + \Delta X_i - X_0) + R_{32}(Y_i + \Delta Y_i - Y_0) + R_{33}(Z_i + \Delta Z_i - Z_0)} \\ y_i' &= -c\frac{R_{21}(X_i + \Delta X_i - X_0) + R_{22}(Y_i + \Delta Y_i - Y_0) + R_{23}(Z_i + \Delta Z_i - Z_0)}{R_{31}(X_i + \Delta X_i - X_0) + R_{32}(Y_i + \Delta Y_i - Y_0) + R_{33}(Z_i + \Delta Z_i - Z_0)} \end{aligned} \quad (1)$$

where $c$ is the focal length, $(X_0, Y_0, Z_0)$ is the projection center, and $R_{mn}, m = 1,2,3, n = 1,2,3,$ are the elements of a rotation matrix giving the orientation of the camera with respect to the object coordinate system. Equations 1 are multiplied by the denominator and the terms are rearranged yielding two linear equations in three unknowns $\Delta X_i, \Delta Y_i, \Delta Z_i$ for each $i = 1,\ldots,N$. More specifically, these equations are given by (cf. Kraus, 1996, p. 49)

$$\begin{aligned} (x_i' R_{31} + cR_{11})\Delta X_i + (x_i' R_{32} + cR_{12})\Delta Y_i + (x_i' R_{33} + cR_{13})\Delta Z_i + x_i' \tilde{Z}_i + c\tilde{X}_i = 0 \\ (y_i' R_{31} + cR_{21})\Delta X_i + (y_i' R_{32} + cR_{22})\Delta Y_i + (y_i' R_{33} + cR_{23})\Delta Z_i + y_i' \tilde{Z}_i + c\tilde{Y}_i = 0 \end{aligned} \quad (2)$$

where

$$\begin{pmatrix} \tilde{X}_i \\ \tilde{Y}_i \\ \tilde{Z}_i \end{pmatrix} = R \begin{pmatrix} X_i - X_0 \\ Y_i - Y_0 \\ Z_i - Z_0 \end{pmatrix} \quad (3)$$

is the object point *i* transformed to the camera coordinate system according to the known exterior orientation of the camera. If we have two or more images taken from different viewpoints, then each new image, where the point is visible, brings two equations more and the unknown deformations at each point can be solved by the traditional method of bundle adjustment. For a single image or weak imaging geometry, some more information is needed to solve the problem. We consider the case where the deformation can be expressed with the help of shape functions *f, g, h* depending on parameter vectors ***a***, ***b***, ***d*** as

$$\begin{aligned} \Delta X_i &= f(X_i, Y_i, Z_i; \boldsymbol{a}) \\ \Delta Y_i &= g(X_i, Y_i, Z_i; \boldsymbol{b}) \\ \Delta Z_i &= h(X_i, Y_i, Z_i; \boldsymbol{d}) \end{aligned} \quad (4)$$

for $i = 1,\ldots,N$. The shape functions are typically polynomials of $X_i, Y_i, Z_i$ and the parameters are the coefficients of the polynomial terms. In this case, the shape functions depend linearly on the parameters, the values of which can be solved from Eqs. 2 using linear least squares techniques. If the shape functions depend nonlinearly on the parameters, then the iterative

Levenberg-Marquardt algorithm is applied because of its good convergence properties for nonlinear least squares problems. For one or more images, the merit function to be minimized is then given by

$$F(\boldsymbol{a},\boldsymbol{b},\boldsymbol{d}) = \sum_{k=1}^{K}\sum_{i=1}^{N} w_{ik}((u_{ik}(x_{ik}', X_i, Y_i, Z_i; \boldsymbol{a},\boldsymbol{b},\boldsymbol{d}))^2 + (v_{ik}(y_{ik}', X_i, Y_i, Z_i; \boldsymbol{a},\boldsymbol{b},\boldsymbol{d}))^2)/(2S) \qquad (5)$$

where $K$ is the number of images, $(x_{ik}', y_{ik}')$ is the observed image point of the $i^{\text{th}}$ object point after deformation in the $k^{\text{th}}$ image, $w_{ik}$ is a nonnegative weight, $S = \sum_{k=1}^{K}\sum_{i=1}^{N} w_{ik}$ , and $u_{ik}$ and $v_{ik}$ are given by (cf. Eq. 2)

$$u_{ik}(\boldsymbol{a},\boldsymbol{b},\boldsymbol{d}) = (x_{ik}' R_{31}^k + c_k R_{11}^k) f(\boldsymbol{a}) + (x_{ik}' R_{32}^k + c_k R_{12}^k) g(\boldsymbol{b}) + (x_{ik}' R_{33}^k + c_k R_{13}^k) h(\boldsymbol{d}) + x_{ik}' \tilde{Z}_{ik} + c_k \tilde{X}_{ik}$$
$$v_{ik}(\boldsymbol{a},\boldsymbol{b},\boldsymbol{d}) = (y_{ik}' R_{31}^k + c_k R_{21}^k) f(\boldsymbol{a}) + (y_{ik}' R_{32}^k + c_k R_{22}^k) g(\boldsymbol{b}) + (y_{ik}' R_{33}^k + c_k R_{23}^k) h(\boldsymbol{d}) + y_{ik}' \tilde{Z}_{ik} + c_k \tilde{Y}_{ik}$$

where $(\tilde{X}_{ik}, \tilde{Y}_{ik}, \tilde{Z}_{ik})$ is the object point $i$ transformed to the camera coordinate system of the $k^{\text{th}}$ image according to Eq. 3 with known rotation matrix $R^k$ and projection center of the $k^{\text{th}}$ camera, and finally $c_k$ is the known focal length of the $k^{\text{th}}$ camera. The weight $w_{ik}$ may be set inversely proportional to the variance of image measurements at $(x_{ik}', y_{ik}')$ and it is zero if point $i$ is not visible in image $k$. In the experiments in the following section, we set all the weights equal to one for simplicity. Once optimal values for the parameters have been found, the deformations can be evaluated using Eq. 4.

The covariance matrix of the estimated parameters is given by the inverse of the coefficient matrix of the normal equations multiplied by the reference variance in the case of linear least squares minimization (Mikhail, 1976, p. 116) while in the Levenberg-Marquardt method, it is characterized by twice the inverse of the Hessian matrix of the merit function minimized (Press *et al.*, 2007, p. 802). The covariance matrix of the 3-D deformations is then obtained through first order error propagation from the covariance matrix of the estimated parameters using the functional dependencies of the deformations on the parameters as described by the shape functions in Eq. 4. The mean precision of the 3-D deformations is given by the square root of the trace of the covariance matrix divided by three times the number of points (Mikhail, 1976, p. 64). In addition to precision estimation, we evaluate the accuracy of the estimated 3-D deformation by computing the root mean squared distance between the estimated deformation and known true deformation at the data points in various test cases with synthetic data in the following section.

## 3. EXPERIMENTS

### 3.1 Single image

The proposed method was first tested with a single image using synthetic data illustrated in Fig. 1. A rectangular grid of data points originally from a horizontal plane $Z = 0$ in an object coordinate system and covering an area of 10×10 m$^2$ was deformed so that the $Z$ coordinates were deformed by a bivariate polynomial of fourth degree, and the $X$ and $Y$ coordinates by a sine function as follows

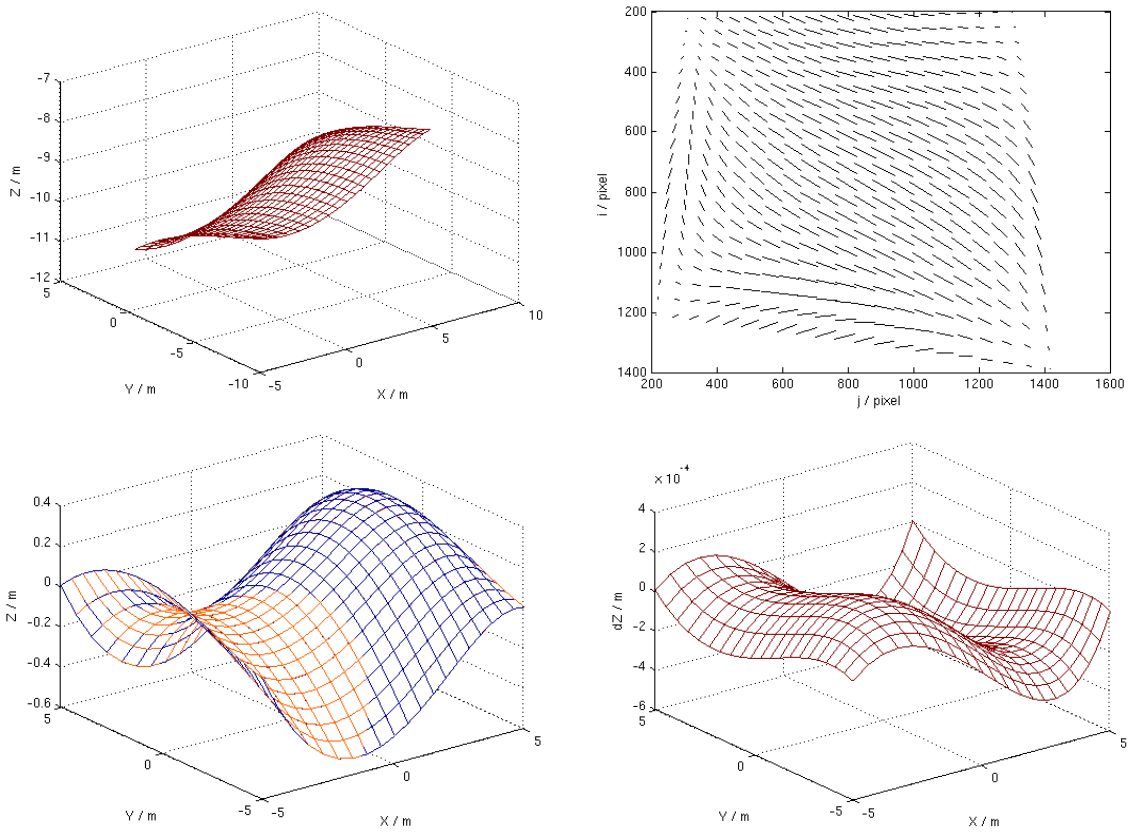


*Figure 1. Deformed surface in the camera centered coordinate system (upper left figure), changes in the image coordinates (upper right figure), estimated (red) and true (blue) deformed surface in the object coordinate system (lower left figure), and difference in Z between the estimated and true deformation (lower right figure). Note that the scales are different in the Z axes (meters versus $10^{-4}$meters).*

$$\begin{aligned} \Delta X_i &= a_0 \sin(\pi(X_i + 5)/10) \\ \Delta Y_i &= b_0 \sin(\pi(Y_i - 5)/10) \\ \Delta Z_i &= d_0(X_i - 5)(X_i + 5) + d_1(Y_i - 5)(Y_i + 5) + d_2(X_i - 5)^2(X_i + 5) \\ &\quad + d_3(Y_i - 5)(Y_i + 5)^2 + d_4(X_i - 5)(X_i + 5)(Y_i - 5)(Y_i + 5) \end{aligned} \tag{6}$$

where $a_0, b_0, d_0, ..., d_4$ are the parameters the values of which were to be estimated. Note that the deformation in Eq. 6 keeps the four corner points of the area fixed in the original positions. The projection center of the camera was located at (-1,0,10) meters in the object coordinate system and the camera was rotated first by 10 degrees around the *X* axis and then by 10 degrees around the *Y* axis in a coordinate system centered at the projection center, from a directly downward looking orientation. The focal length of the camera was 10 mm, the principal point located in the middle of the image, the image was assumed to be free of lens distortions, and the pixel size of the image was 10×10 μm$^2$. With these settings, the image coordinates of the deformed 3-D points were then calculated with zero mean and standard deviation of 0.1 pixels normally distributed noise added to the image measurements. The unknown values of the seven parameters of the shape functions were estimated from the deformed image measurements and the 3-D points before deformation. The estimated deformation fits well in with the true deformation. The maximum difference between the estimated and true deformation is less than 0.5 mm in the *Z* direction when the distance between the camera and the object is about 10 m with the given

configuration described above. This example thus shows that the method may work even with a single image.

It was then studied how the accuracy and precision of the proposed method depend on the precision of image observations. Hundred trials were carried out with zero mean and variable standard deviation $\sigma$ of noise added to the image observations. The results in Table 1 show that the dependencies are approximately linear and the accuracy and mean precision achieved are very high. The object, deformation, and camera setup were the same as in Fig. 1.

*Table 1. RMSE and mean precision of the 3-D deformation estimated by the proposed method at the data points as a function of noise added to the image observations.*

| *Standard deviation σ of noise (pixel)* | *RMSE (mm) proposed method* | *Mean precision (mm) proposed method* |
|---|---|---|
| *0.01* | *0.025* | *0.015* |
| *0.05* | *0.11* | *0.076* |
| *0.1* | *0.25* | *0.15* |
| *0.5* | *1.2* | *0.76* |
| *1* | *2.5* | *1.5* |

*Table 2. RMSE and mean precision of the 3-D deformation estimated by the proposed method at the data points as a function of number of points ($\sigma$ = 0.1 pixel).*

| *Number of points* | *RMSE (mm) proposed method* | *Mean precision (mm) proposed method* |
|---|---|---|
| *2*2 = 4* | *3.1* | *2.5* |
| *3*3 = 9* | *1.9* | *1.1* |
| *4*4 = 16* | *1.4* | *0.83* |
| *6*6 = 36* | *0.81* | *0.51* |
| *11*11 = 121* | *0.45* | *0.28* |
| *21*21 = 441* | *0.25* | *0.15* |
| *41*41 = 1681* | *0.13* | *0.079* |
| *81*81 = 6561* | *0.066* | *0.040* |

The accuracy and precision of the proposed method depend also on the number and density of data points. This was investigated by changing the cell size in the grid of data points covering the same object area as in Fig. 1. Each object point provided two observation equations (one for $x_i'$ and one for $y_i'$) so that the minimum number of points necessary was half of the number of parameters to be estimated. In this test data, there were seven parameters (cf. Eq. 6) and thus the minimum of four points was necessary. The results in Table 2 show that the estimation is possible from only four points while the accuracy and mean precision increase as the number and density of points increase. In the case of four points, the points were not the corner points of the area (which would have remained fixed) but inside the area being deformed. The noise level in the image observations was 0.1 pixel and the mean precision values and the RMSE values of the

estimated deformation with respect to the known true deformation at the data points have been averaged over hundred trials.

The performance of the proposed method in a nonlinear case was investigated by generating test data, where the $Z$ coordinates of the same target and imaging configuration as above were deformed by a two-dimensional Gaussian function with three parameters describing the amplitude and $X$ and $Y$ spreads of the bell shape. The center position of the bell shape was regarded as known. A set of initial values for the parameters were generated by perturbing the true values of the parameters by shifts derived from a normal distribution of zero mean and variable standard deviation. The same standard deviation of shifts was used for all the three parameters as the true values of these parameters were selected to be of the same order of magnitude. Hundred trials were performed for each standard deviation of shifts. The results in Table 3 show that 100 per cent convergence is achieved when the relative difference between the initial and true values of the parameters is less than 13 per cent for this imaging configuration. The RMS distance between the estimated and true deformation is less than 0.5 mm, when the noise added to the image observations is zero mean and standard deviation of 0.1 pixel.

*Table 3. Number of successful trials and RMSE of the 3-D deformation estimated by the proposed method at the data points as a function of relative difference between the initial and true values of the parameters of the shape function on the average ($\sigma$ = 0.1 pixel).*

| *Standard deviation of shifts added to true parameters* | *Relative difference between initial and true parameters (%)* | *Number of successful trials (%)* | *RMSE (mm) proposed method* |
|---|---|---|---|
| *0.01* | *0.6* | *100* | *0.48* |
| *0.05* | *3.0* | *100* | *0.47* |
| *0.1* | *6.5* | *100* | *0.45* |
| *0.2* | *13* | *100* | *0.47* |
| *0.3* | *20* | *98* | *0.46* |
| *0.4* | *26* | *93* | *0.48* |
| *0.5* | *33* | *84* | *0.47* |
| *1* | *70* | *66* | *0.44* |
| *5* | *320* | *14* | *3400* |

## 3.2 Weak imaging geometry

A synthetic data set with weak imaging geometry was generated, including four cameras located near each other and monitoring a planar surface, which was deformed by polynomials and sine functions as in Eq. 6 above. The deformation was estimated using the traditional method and the proposed one. The results illustrated in Fig. 2 show that the traditional method gives mostly noise while the proposed method is able to estimate the deformation very accurately. The RMS distance between the estimated and true deformation is 0.2 mm for the proposed method and 400 mm for the traditional one.

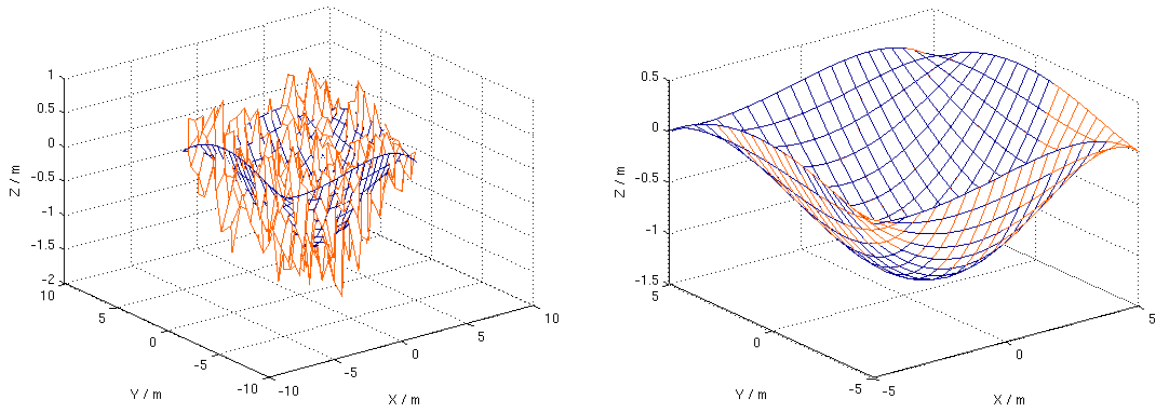


*Figure 2. True deformed surface in blue and estimated deformed surface in red given by the traditional method (left figure) and by the proposed method (right figure).*

A series of experiments was carried out with increasing distance between the projection centers of the four cameras and thus with improving imaging geometry. The projection centers of the cameras were located equidistantly on the circumference of a circle of radius *s* on a plane at a distance of 10 m oriented to the object. The rotation angles of the exterior orientations were zeros. Hundred trials were performed for each setup of cameras with noise of zero mean and standard deviation of 0.1 pixel added to the image observations. The mean precisions and RMS distances between the estimated and true deformation on the average are presented in Table 4. The results show that the proposed method provides high accuracy and mean precision for all setups while the accuracy and mean precision of the traditional method decrease dramatically as the imaging geometry becomes weaker, i.e., when *s* decreases as could be expected.

*Table 4. RMSE and mean precision of the 3-D deformation estimated by the proposed and traditional method at the data points as a function of distance between four cameras (see text for explanation of s, $\sigma$ = 0.1 pixel).*

| | | *Proposed method* | | *Traditional method* | |
|---|---|---|---|---|---|
| *s (m)* | *2s / depth* | *RMSE (mm)* | *Mean precision (mm)* | *RMSE (mm)* | *Mean precision (mm)* |
| *0.001* | *0.0002* | *0.14* | *0.09* | *6700* | *1600* |
| *0.005* | *0.001* | *0.15* | *0.09* | *1200* | *640* |
| *0.01* | *0.002* | *0.14* | *0.09* | *560* | *320* |
| *0.05* | *0.01* | *0.15* | *0.09* | *110* | *65* |
| *0.1* | *0.02* | *0.14* | *0.09* | *55* | *32* |
| *0.5* | *0.1* | *0.14* | *0.09* | *11* | *6.5* |
| *1* | *0.2* | *0.14* | *0.09* | *5.6* | *3.3* |
| *5* | *1* | *0.09* | *0.05* | *1.3* | *0.8* |

The accuracy and mean precision of the proposed method was further evaluated as a function of number of cameras for weak (*s* = 0.001 m) and strong (*s* = 5 m) imaging geometry. The results averaged over hundred trials are shown in Table 5. It may be concluded that the accuracy and mean precision increase when we have more cameras and also when the imaging geometry is

improved. In this experiment, the setups of one, two, and three cameras were generated by removing cameras from the setup of four cameras so that the base was equal to 2*s* in the case of two cameras while in the case of three cameras, the cameras were located in the corners of a right-angled triangle with a hypotenuse equal to 2*s*.

*Table 5. RMSE and mean precision of the 3-D deformation estimated by the proposed method at the data points as a function of number of cameras ($\sigma$ = 0.1 pixel).*

| *Number of cameras* | *s (m)* | *2s / depth* | *RMSE (mm) proposed method* | *Mean precision (mm) proposed method* |
|---|---|---|---|---|
| *1* | *0.001* | *0.0002* | *0.29* | *0.18* |
| *2* | *0.001* | *0.0002* | *0.22* | *0.13* |
| *3* | *0.001* | *0.0002* | *0.16* | *0.10* |
| *4* | *0.001* | *0.0002* | *0.15* | *0.09* |
| *1* | *5* | *1* | *0.24* | *0.15* |
| *2* | *5* | *1* | *0.13* | *0.08* |
| *3* | *5* | *1* | *0.10* | *0.06* |
| *4* | *5* | *1* | *0.09* | *0.05* |

In the case of four cameras and 441 object points, the CPU time varied from 0.01-0.05 seconds for the proposed method while for the traditional method, it was 0.16-0.25 seconds in a HP ProLiant DL785 G5 server of CSC - IT Center for Science. The reconstruction of the 3-D object coordinates after deformation including the inversion of a 3×3 matrix for each point takes most of the computing time in the traditional method. The inversion of only one matrix of size of the number of parameters is needed in the proposed method which makes it very fast and suitable for real time applications.

### 3.3 Real data

Real data testing was carried out with two calibrated cameras monitoring a plate with 24 circular target points attached on it as illustrated in Fig. 3. The ratio of the base to mean distance to the object was 0.62 for this imaging geometry. A deformation was caused on the plate by turning two screws fixed to the middle of the plate and to the upper edge of the plate, respectively. The image coordinates of the target points and stable red and green points behind the plate were measured as center points of the circular targets before and after deformation using iWitness software. The 3-D coordinates of the target points were also provided by iWitness and the 3-D deformation based on the traditional method was calculated for the reference. A correct scale for the 3-D measurements was obtained by a known distance between two stable target points next to the plate. Using the standard deviations of the 3-D coordinates given by iWitness before and after deformation, the mean precision of the reference deformation was evaluated to be 0.19 mm. The deformed surface and the deformation in the direction of the optical axis of the left camera are shown in blue in Fig. 4. The coordinate system follows here the convention of iWitness so that the system is centered at the left camera, *X*-axis points to the right, *Y*-axis to the target (direction of the optical axis), and *Z*-axis upwards.

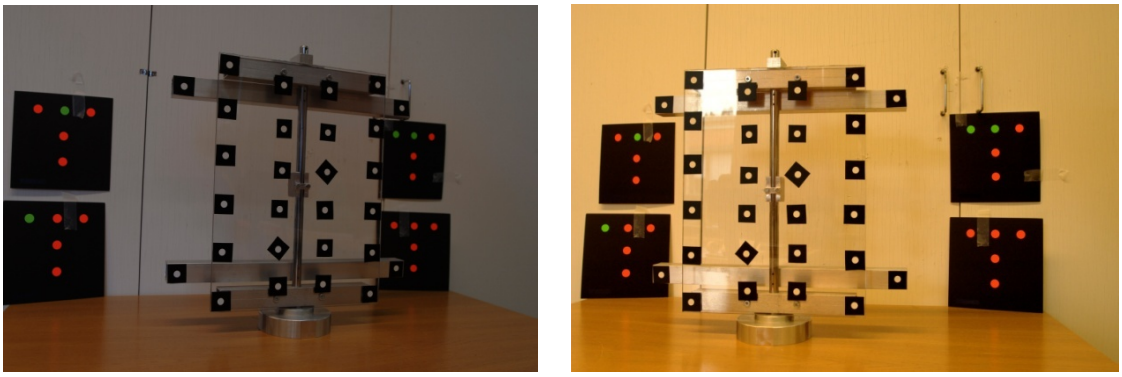

*Figure 3. Left and right images of a plate.*

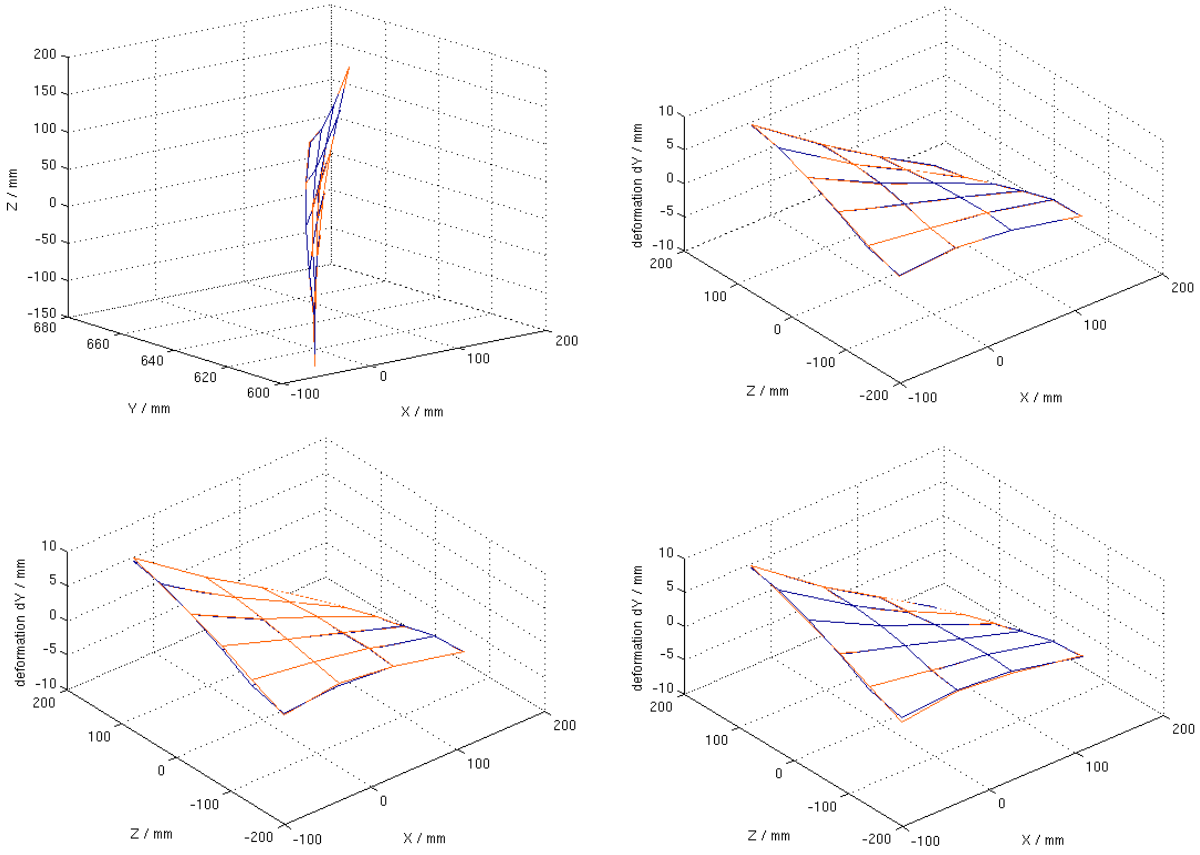


*Figure 4. Deformed surface reconstructed using the proposed method in red and the traditional method in blue (upper left figure). Deformation in the direction of the left optical axis estimated using both images (upper right figure), only the left image (lower left figure), and only the right image (lower right figure). The deformations in red are according to the proposed method and the deformations in blue are according to the traditional method using both images.*

The proposed method was then applied using bivariate polynomials of second degree in $X$ and $Z$ as shape functions to model the deformations in the $X$ and $Z$ directions and a bivariate polynomial of fourth degree in $X$ and $Z$ to model the deformation in the $Y$ direction with all the 27 coefficients of the polynomial terms as parameters. In the first test, the image observations in both the left and right images were used and the 3-D object coordinates before deformation were those computed previously by the traditional method. The results in Fig. 4 (upper figures) show

that the proposed method yields similar deformation as the traditional one. The RMS distance is 0.14 mm between the deformed surfaces computed by the proposed and traditional methods. The mean precision of the deformation estimated by the proposed method is 0.14 mm, taking into account also the uncertainties in the reference 3-D coordinates before deformation.

The proposed method was then tested using only a single image, i.e., either the left or right image. Using the same polynomial shape functions as for the case of two images, did not yield satisfactory results. Consequently, the number of terms in the polynomials and thus the number of parameters to be estimated was reduced so that those terms were left out, the coefficients of which were small in the two image case. The deformation in the $Y$ direction was thus modeled by a bivariate polynomial of second degree in $X$ and $Z$ and the deformations in the $X$ and $Z$ directions were modeled by bivariate polynomials of first degree in $X$ and $Z$ and a mixed term of $X$ times $Z$ (in the $X$ direction only). The results in Fig. 4 (lower figures) prove that the deformation can be estimated from a single image. The RMS distances to the reference surface are 0.44 mm and 0.35 mm as estimated using only the left or right image, respectively. The corresponding mean precisions of the deformations estimated by the proposed method are 0.17 mm and 0.16 mm.

## 4. CONCLUSIONS

Estimation of 3-D deformation from a single image or from multiple images with weak imaging geometry was studied. The ill-posed problem was solved by incorporating additional information on the shape of deformation that is expected to occur. The parameters of the shape functions were solved from image observations after deformation and known reference shape of the object before deformation without any need of reconstructing the 3-D object coordinates after deformation. Consequently, the computing time was lower for the proposed method than for the traditional one. Due to fast computing time, the proposed method might be used for real time applications.

Testing with synthetic data proved that the accuracy and mean precision of the proposed method are much higher than of the traditional method even for strong imaging geometry if the shape functions are correctly selected. The accuracy and mean precision of the proposed method depended approximately linearly on the uncertainty of image observations. For a realistic noise level of 0.1 pixels in the image observations, an accuracy of about 1:57000 and a mean precision of about 1:94000 of the object dimensions were achieved with a single image and synthetic data of 441 points. The method worked for a minimal number of four points to estimate the values of seven parameters while the accuracy and mean precision of the method improved as the number and density of the points increased. Although the method worked very well for a single image and weak imaging geometry of multiple images, somewhat higher accuracy and mean precision were achieved when more images were involved and when the imaging geometry was stronger. The convergence of the method was good in a test case where the shape function depended nonlinearly on the parameters. In the real data experiment, the deformation of a plate could be estimated with an accuracy of about 1:1000 and a mean precision of about 1:2200 of the object dimensions using only a single image. Future research includes more studies on cases where the correct functional forms of the shape functions are not known.

## 5. REFERENCES


Albert, J., Maas, H.-G., Schade, A., and Schwarz, W., 2002. Pilot studies on photogrammetric bridge deformation measurement, Proc. 2nd IAG Commission IV Symposium on Geodesy for Geotechnical and Structural Engineering, Berlin, May 21-24, 2002, pp. 133-140.

Chen, Y., Kim, T.-K., and Cipolla, R., 2010. Inferring 3D shapes and deformations from single views, Lecture Notes in Computer Science, Vol. 6313, Proc. 11th European Conference on Computer Vision, Crete, September 5-11, 2010, pp. 300-313.

Fraser, C.S. and Riedel, B., 2000. Monitoring the thermal deformation of steel beams via vision metrology, ISPRS Journal of Photogrammetry and Remote Sensing, Vol. 55, Issue 4, pp. 268-276.

Hinz, S., Stephani, M., Schiemann, L., and Rist, F., 2007. Automatic reconstruction of shape evolution of ETFE-foils by close-range photogrammetric image analysis, International Archives of Photogrammetry, Remote Sensing and Spatial Information Sciences, 36 (3/W49B), PIA07 - Photogrammetric Image Analysis, Munich, September 19-21, 2007, pp. 59-63.

Jiang, R. and Jauregui, D.V., 2010. Development of a digital close-range photogrammetric bridge deflection measurement system, Measurement, Vol. 43, Issue 10, pp. 1431-1438.

Kraus, K. mit Beiträgen von Jansa, J. und Kager, H., 1996. Photogrammetrie – Verfeinerte Methoden und Anwendungen, Band 2, Dümmler Verlag, Bonn, 495 p.

Leotta, M.J., 2010. Generic, Deformable Models for 3-D Vehicle Surveillance, Ph.D. thesis, Brown University, 250 p.

Liu, J.-W., Liang, J., Liang, X.-H., and Tang, Z.-Z., 2010. Videogrammetric system for dynamic deformation measurement during metal sheet welding processes, Optical Engineering, Vol. 49, No. 3, 033601, 8 p.

Maas, H.-G., 1998. Photogrammetric techniques for deformation measurements on reservoir walls, IAG SC4 Symposium Geodesy for Geotechnical and Structural Engineering, Eisenstadt, April 20-22, 1998, 6 p.

Mikhail, E.M. with contributions by Ackermann, F., 1976. Observations and Least Squares, Harper & Row, Publishers, 497 p.

Orteu, J.-J., 2009. 3-D computer vision in experimental mechanics, Optics and Lasers in Engineering, Vol. 47, Issue 3-4, pp. 282-291.

Peipe, J., Reinking, J., and Schneider, C.-T., 2006. Photogrammetric 3-D digitizing for deformation analysis - new developments and applications, 3rd IAG Symposium on Geodesy for Geotechnical and Structural Engineering / 12th FIG Symposium on Deformation Measurement, Baden, May 22-24, 2006, 9 p.

Press, W.H., Teukolsky, S.A., Vetterling, W.T., and Flannery, B.P., 2007. Numerical Recipes: The Art of Scientific Computing, Third Edition, Cambridge University Press, New York, 1235 p. + xxi.

Taddei, P. and Bartoli, A., 2008. Template-based paper reconstruction from a single image is well posed when the rulings are parallel, IEEE Computer Society Conference on Computer Vision and Pattern Recognition Workshops, Anchorage, June 23-28, 2008, pp. 1-6.

Tournas L., Tsakiri M., and Kattis M., 2006. Displacement monitoring at the micron level using digital photogrammetry, 3rd IAG Symposium on Geodesy for Geotechnical and Structural Engineering / 12th FIG Symposium on Deformation Measurement, Baden, May 22-24, 2006, 9 p.

Tyson, J., Schmidt, T., and Galanulis, K., 2002. Biomechanics deformation and strain measurements with 3D image correlation photogrammetry, Biomechanics Series: Part 3, pp. 39-42.